Creep behaviour of injection moulded polyamide 6/organoclay nanocomposites by nanoindentation and cantilever-bending

Rocio Seltzer [a,*], Yiu-Wing Mai [a], Patricia M. Frontini [b]

[a] Center for Advanced Materials Technology (CAMT), School of Aerospace, Mechanical and Mechatronic Engineering, The University of Sydney, Sydney, Australia
[b] Instituto de Investigaciones en Ciencia y Tecnología de Materiales (INTEMA), Departamento de Materiales, Universidad de Mar del Plata, Mar del Plata, Argentina

ARTICLE INFO

ABSTRACT

The creep behaviour of injection moulded PA 6/organoclay nanocomposites was studied by depth-sensing nanoindentation and DMA cantilever-bending. The glass transitions of PA 6 and its nanocomposites were decreased below room temperature upon saturation with water so that the materials could be tested in the rubbery regime. For nanoindentation creep on the skin and core regions of injection moulded samples, whilst organoclay improves the creep resistance of PA 6, the enhancement is due to the decrease of the initial compliance at zero time but the time-dependent creep is actually increased. In contrast, for cantilever-bending creep, organoclay reduces the creep compliance and the time-dependent creep in PA 6. It is suggested that the organoclay imparts a constraint effect on the PA 6 molecular chains, restricting their mobility in the bulk compared to the surface and hence improving their resistance to creep. A modified Halpin–Tsai equation was used to model their creep behaviour under these two loading configurations and compared to experimental data.

© 2011 Elsevier Ltd. All rights reserved.

1. Introduction

Advances in polymer technology are making it possible to produce plastic parts that were traditionally made from metals. In particular, Polyamide 6 (or Nylon 6) is widely used in the automotive industry due to its good surface appearance, wear, chemical and heat resistance. However, like most other polymers, PA 6 creeps even at room temperature which reduces its applicability in load-bearing components. Organoclay, a commonly used nano-filler, has shown to influence the viscoelastic response of some polymers [1–3] including PA 6 [4].

At low loads, polymers display elastic, viscoelastic or viscous behaviour depending on the temperature and loading rate. The solid and melt properties of PA 6/clay nanocomposites have been widely studied (e.g. [5–9]). It is concluded that organoclay enhances the elastic modulus due to the high aspect ratio and stiffness of the particles [10] but not the constraint of the polymer molecules imposed by the nanoclay. However, this constraint effect, founded on the fact that the thickness of the clay platelets approaches the length scale of a single polymer coil, does play a role in the regime of viscous flow, where the viscosity is highly increased compared to their micro-particles counterpart [11]. This

is thought to be caused by the small size and high surface area of the clay platelets, together with the short inter-particle distance which prevents free-rotation of the matrix molecules [12].

Between its glass transition and melting temperatures (T_g and T_m, respectively), PA 6 is in a rubber-like state, where long-range segmental motion is occurring but the thermal energy is insufficient to overcome entanglement interactions that inhibit flow. It is expected that, in this intermediate rubbery regime, the organoclay also acts at a molecular level reducing the viscoelastic flow. The rubbery regime can be achieved by increasing the temperature, but also by increasing the moisture content [13,14]. According to Reimschuessel's [15] results, the T_g of dry PA 6 can be lowered from 41.5 °C to −13 °C by saturation with water. This allows for the viscoelastic properties of rubbery PA 6 to be tested at room temperature. Vlasveld et al. [4] investigated the viscoelastic response of dry PA 6/organoclay at room temperature and showed some preliminary results on creep tests performed at 80 °C and on water-conditioned samples. Apparently, the organoclay is more effective in reducing the creep compliance in the rubbery plateau (either at high temperature or under moisture conditions) than in the glass transition region. Encouraged by these findings, we have studied in-depth the viscoelastic properties of PA 6/organoclay nanocomposites in the rubbery plateau with water-saturated samples.

Injection moulded PA 6/organoclay nanocomposites possess a skin-core structure [16,17] and, consequently, the resulting mechanical responses in the skin and core regions are different

[18,19]. Hence, the local distinctive effect of organoclay addition on the viscoelastic properties in both regions was studied using nanoindentation. The creep compliance was determined from the indentation results following a procedure[1] proposed by Seltzer and Mai [20]. The advantage of this procedure with respect to other methods [21–23] is that it separates the viscoelastic from the plastic response, both of which unavoidably occur simultaneously due to the geometry of the indentation test. In addition, the creep compliances of bulk materials were also investigated using cantilever beams under bending in the Dynamic Mechanical Analyzer (DMA) and compared to the nanoindentation results.

This paper continues our previous work[2] [19], where the differences in the skin and core morphology and quasistatic properties of PA6/organoclay nanocomposites were elucidated. However here, the aim is to examine, quantify and model the creep response of water-saturated injection moulded specimens of PA 6 nanocomposites under both nanoindentation and cantilever-bending loads. The difference between surface creep and bulk creep behaviour will also be evaluated.

2. Experimental work

2.1. Material

Polyamide 6 (Akulon F 232-D) was obtained from DSM Engineering Plastics and the organoclay used was Cloisite® 30B supplied by Southern Clay Products Inc. through Jim Chambers & Associates, Australia. It was organically modified with alkyl ammonium surfactant, namely, methyl, tallow, bis-2-hydroxyethyl quartenary ammonium chloride, having a cation exchange capacity of 90 mequiv/100 g. All samples were dried in a vacuum oven at 80 °C for 24 h before melt blending. A range of PA 6/organoclay nanocomposites containing 0, 1.1, 2.2, 3.3 and 4.5 vol.% organoclay (denoted by N0.0, N1.1, N2.2, N3.3 and N4.5, respectively) were prepared by melt compounding using a ZSK 30 twin-screw extruder and injected to dumb-bells and rectangular bars for mechanical testing.

2.2. Dynamic mechanical analysis

A dynamic mechanical analyser DMA 2980, TA Instruments, was used to study the molecular relaxations and bulk creep compliances of PA 6 and its nanocomposites. The DMA was used in the single-cantilever mode. Specimens were cut from the narrow part of the tensile dumb-bells and their dimensions were $40 \times 10 \times 3$ mm^3. The samples were pre-conditioned by either drying in oven at 80 °C for 24 h or submersion in water at 70 °C till the constant mass condition was reached (approximately 3 weeks).

Creep tests were conducted at a stress of 2 MPa for all materials in order to avoid any plastic or viscoplastic deformation. The molecular relaxations were studied using a frequency of 1 Hz over a temperature range of −135 to 150 °C. The constant heating rate was 3 °C/min.

2.3. Nanoindentation

The mechanical responses in the surface (skin) and mid-thickness (core) regions of the injection moulded bars, Fig. 1, were determined by depth-sensing indentation with nano-scale resolution. Indentation measurements were performed using a UMIS nanoindenter manufactured by CSIRO, Australia. Indentation load,
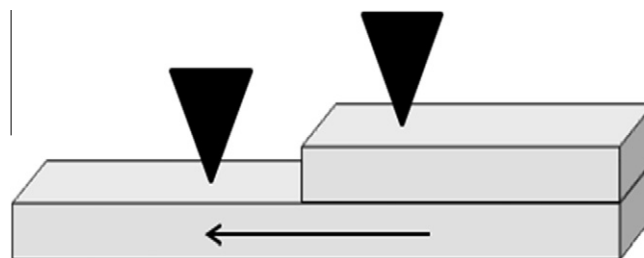

Fig. 1. Schematic of an indentation moulded bar showing the two indentation locations. (The arrow shows the injection flow direction.)

P, and depth, h, were recorded simultaneously for a complete load-hold-unload cycle using a spherical indenter with a radius, R, 20 μm. The contact force for detection of the surface position was 0.05 mN. The maximum load was attained in 5 s. Tests were performed at room temperature in submerged conditions to ensure moisture equilibrium at all times.

The indentation specimens were prepared by immersing the injection moulded bars in water at 70 °C for 3 weeks, and then machining to $1 \times 1 \times 1$ cm^3 prisms. To smooth the surfaces, ∼2 μm were removed using a microtome. Ten indentations separated by a distance of 100 μm were made on the skin and core regions of each sample. The local surface creep compliance J was determined following the procedure developed in [20]. For details, see Appendix A.

3. Results and discussion

3.1. Molecular relaxations

Table 1 shows the equilibrium water content of the PA 6 nanocomposites calculated relative to the matrix mass, which is the only permeable phase. All materials have reached similar equilibrium values independent of the clay loading. These results show that although organoclay affects water permeability [24] it does not influence the water uptake capacity of PA 6 in the range of clay loading studied.

Fig. 2 shows that the storage moduli of dry and wet PA 6 are increased by the addition of organoclay in the temperature range studied. Evidently, the organoclay is more effective to improving the storage modulus at temperatures above the abrupt drop, i.e., the glass transition temperature T_g. This phenomenon was observed before [10] and was satisfactorily explained by simple micromechanics models. Water decreases T_g and the storage modulus above ∼0 °C owing to its plasticization effect. However, below 0 °C, the storage modulus is increased since water is transformed from liquid to solid.

Fig. 3 show the loss moduli of PA 6 and its clay composites. In the dry samples, Fig. 3a, three distinctive peaks can be recognized, α, β and γ, which belong to the three well-known relaxation processes in PA 6. Upon water-saturation, all α and β peaks are shifted to lower temperatures but the γ-relaxation peak is not visible as it

---

[1] In Eq. (7) of Ref. [20], π should become $\sqrt{\pi}$.
[2] In Eq. (3) of Ref. [19], the indentation modulus is given by: $E = [\sqrt{\pi}(1 - v^2)S/2\sqrt{a}]$.
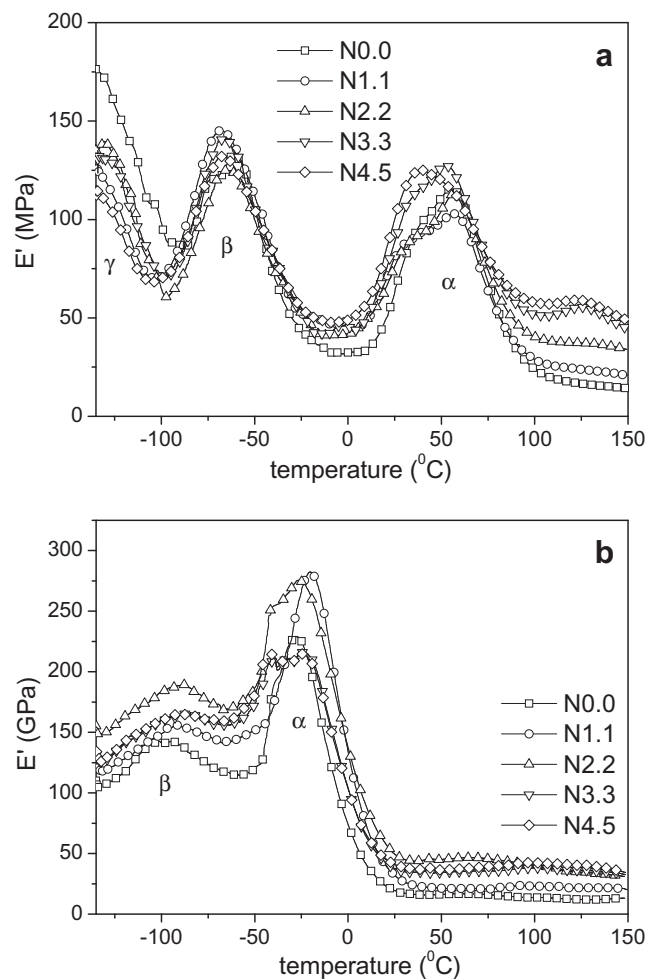
Table 1
Water content at saturation in neat Pa 6 and its nanocomposites.

Material	Water content (wt.%)
N0.0	7.87
N1.1	7.47
N2.2	7.51
N3.3	7.40
N4.5	7.44
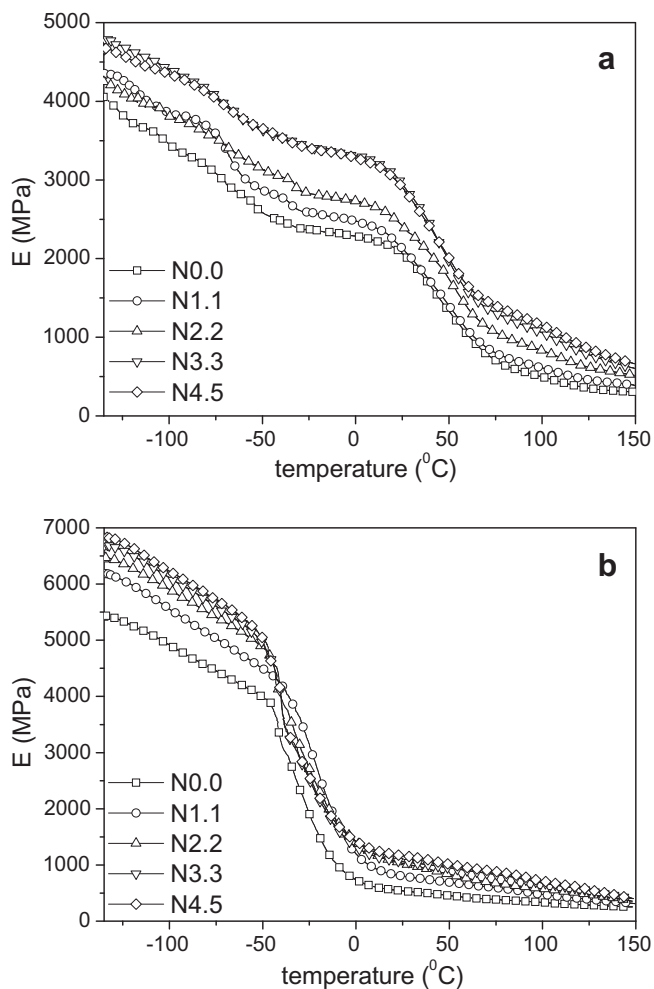
Fig. 2. Storage modulus *vs* temperature of (a) dry and (b) water-saturated PA 6 and its nanocomposites.

Fig. 3. Loss modulus *vs* temperature of (a) dry and (b) water-saturated PA 6 and its nanocomposites showing the α, β and γ relaxations.

is out of the temperature range studied, Fig. 3b. The general trend is that organoclay increases the dissipation energy but the horizontal positions of the peaks remain unchanged.

Fig. 4 shows the loss tangent, which is the ratio between the dissipated and the stored energies. In these two plots, the three relaxation peaks in the dry specimens and the two relaxation peaks in the wet specimens can be identified. The peak value of the α relaxation in the *tan δ* plot is usually considered to be the glass transition temperature (T_g) in PA 6 [25]. It is noted that organoclay barely modifies the T_g of PA 6. In other studies, however, it has been shown that organoclay decreases [26] or increases [27] the T_g of PA 6. These different trends are probably due to the type and quantity of organic modifier used to compatibilize the clay and PA 6. The decrement in T_g by water sorption is well-known in polymers. This shift of T_g can be explained in terms of two main mechanisms: (a) the water molecules screen off the attractive forces between polymer chains and (b) the absorbed water enlarges the free volume amongst polymer chains, allowing the chain segments greater freedom of movement. An important consequence of this decrease of T_g in wet PA 6 and its nanocomposites below 25 °C is that the viscoelastic flow in the rubbery state can be studied at room temperature, which enables the creep experiments to be easily performed.

Creep in polymers is related to their molecular chains mobility. Both the location and magnitude of the glass transition peak reflect the extent of this mobility. While T_g has not been modified by the

organoclay, the value of *tan δ* at the peak steadily decreases with clay loading. This trend indicates that the polymer chain mobility might be decreased in the presence of organoclay particles, and hence the creep resistance could be improved. This hypothesis will be studied in the following sections.

3.2. Viscoelastic response

DMA and indentation creep tests (in the skin and core regions) give a wide perspective of the time-dependent behaviour of these materials since different features affect the mechanical response in each situation. DMA is a macro-mechanical test on the bulk material, where the applied stress field is predominantly unidirectional, while the nanoindentation test is more sensitive to molecular phenomena and the local surface material is under a triaxial stress state. The difference between the indented locations is that the viscoelastic response of PA 6 in the skin region is modified by the high crystallite orientation induced by the organoclay and the orientation of organoclay itself, while in the core region the crystallites are randomly oriented and the organoclay is only oriented with respect to the injection flow direction [19].

Creep compliance (*J*) curves of water-saturated PA 6 and its nanocomposites obtained from the nanoindentation tests are shown in Fig. 5a and b together with the macroscopic creep tests (see Fig. 5c) for comparison. Although the shapes of the *J*(*t*) curves
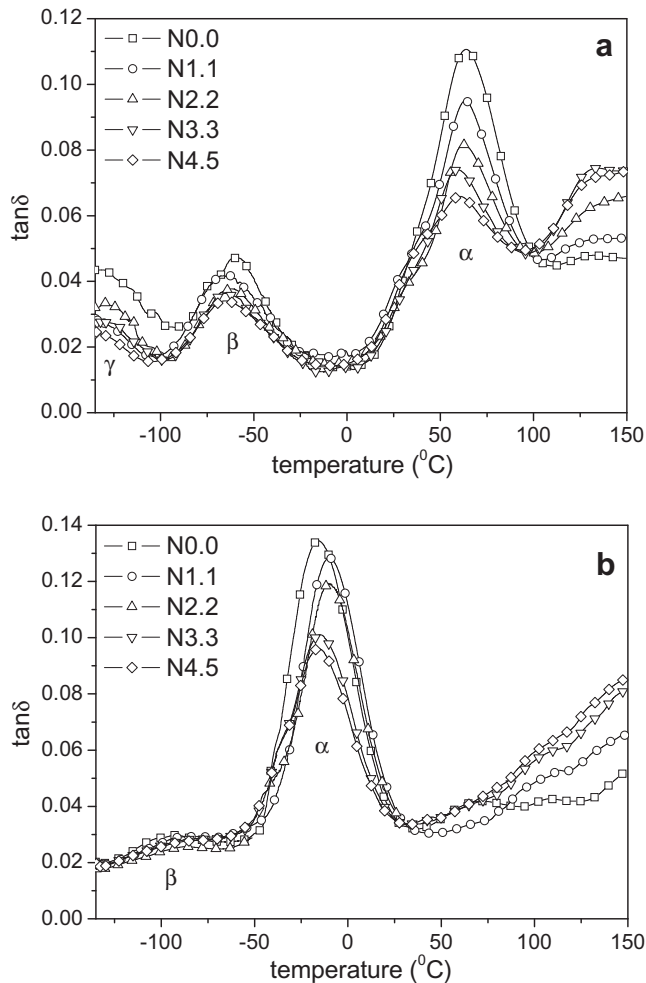
Fig. 4. Loss tangent *vs* temperature of (a) dry and (b) water-saturated PA 6 and its nanocomposites showing the α, β and γ relaxations.

are similar, the position along the *y*-axis, representing the initial compliance at time zero $J(0) = J_0$, differs. The creep compliance values are *lower* in the skin region than in the core region due to the processing orientation effect near the mould walls. In PA 6 there is molecular orientation, and in nanocomposites the crystals and organoclay are also aligned in the injection flow direction [19]. There is no direct relationship between the creep compliances obtained with cantilever-bending and nanoindentation tests since the induced stress states are very different in these two loading geometries. Hence, nanoindentation evaluates the local surface material creep behaviour and cantilever-bending yields an average creep response of the bulk material.

It is clearly shown in Fig. 5 that the incorporation of organoclay shifts the creep compliance curves to lower values illustrating the increase in creep resistance. But two points should be noted. One, the creep compliance $J(t)$ measured consists of an initial compliance J_0 and a time-dependent compliance $(J(t) - J_0)$. To examine the role of organoclay on time-dependent creep, it is necessary to separate these two components. This is discussed in Section 3.3 below. Two, with organoclay loading beyond 3.3 vol.%, no further improvement against creep of PA 6 can be gained. Similar behaviour has also been reported in other studies [10,18]. The two main reasons for this behaviour are the morphological changes induced by organoclay in PA 6 matrix (i.e., promotion of the soft γ-phase [28,29]) and the particle–particle interaction at high filler loading which decreases the matrix–particle load transfer [30].
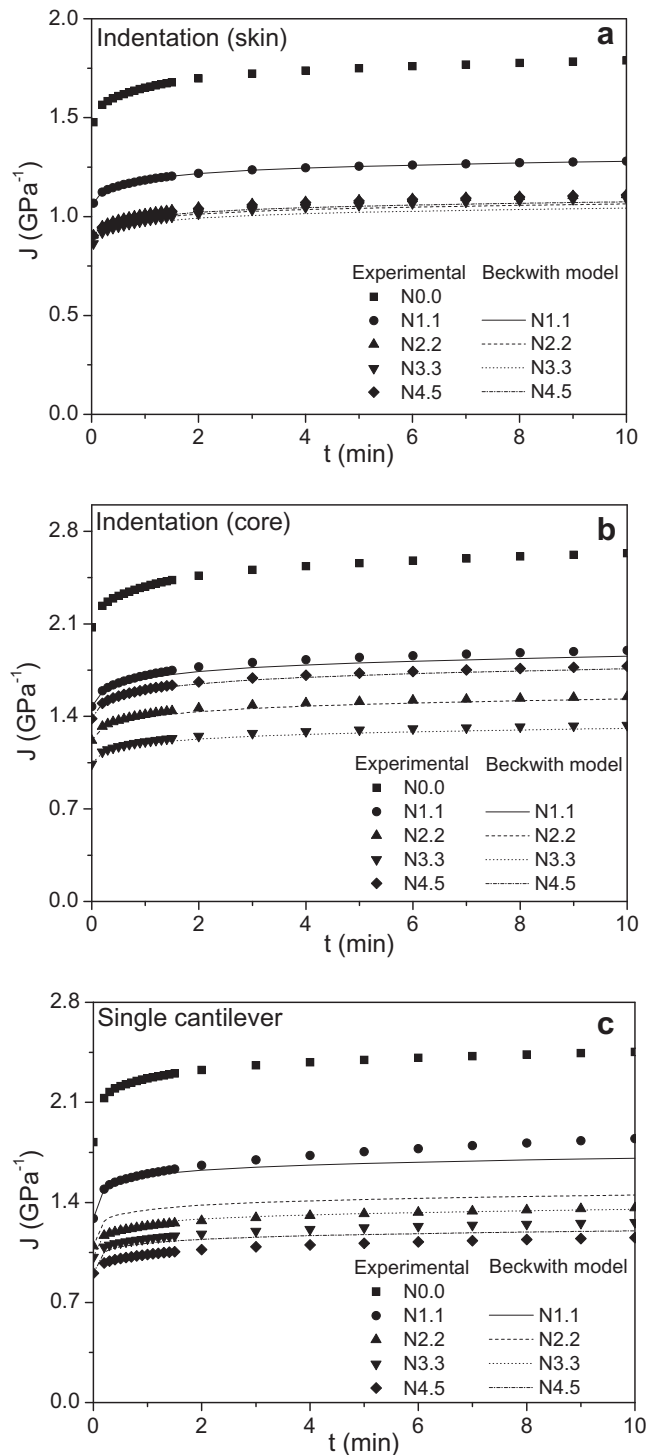

Fig. 5. Comparisons of experimental creep compliance of water-saturated PA 6 and its nanocomposites with Beckwith equation (Eq (1)): (a) nanoindentation on skin region, (b) nanoindentation on core region and (c) cantilever-bending of bulk sample.

3.3. Analyzing creep compliance

To further investigate the role of organoclay on the creep resistance of PA 6, the micro-mechanical model proposed by Halpin–Tsai [31], which has been shown to predict successfully the elastic modulus of polymer-layered nanocomposites [10,32] and modified for time-dependent characterisation by Beckwith [33], is used. That is

Table 2
Experimental (ϕ, J_0) and fitting (ζ) parameter for Beckwith's equation.

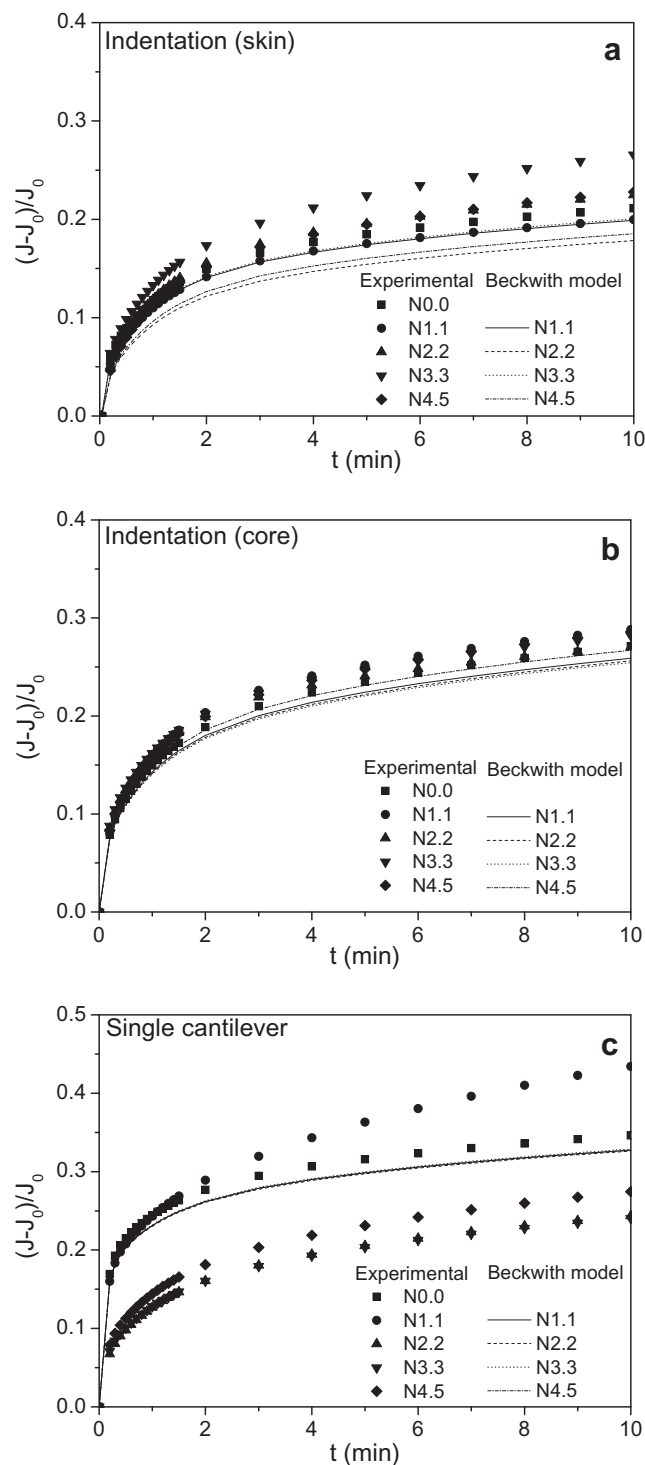| | | Nanoindentation | | | | Single-cantilever-bending | |
| | | Skin | | Core | | | |
	ϕ_f	J_0 (GPa^{-1})	ζ	J_0 (GPa^{-1})	ζ	J_0 (GPa^{-1})	ζ
N0.0	0.0000	1.48	N/A	2.07	N/A	1.82	N/A
N1.1	0.0074	1.07	143	1.47	143	1.29	150
N2.2	0.0150	0.91	116	1.22	117	1.10	112
N3.3	0.0227	0.86	75	1.04	107	1.02	129
N4.5	0.0306	0.90	49	1.38	35	0.91	114

$$J_c(t) = J_m(t) \left[\frac{J_f^{-1}(1 - \phi_f) + J_m(t)^{-1}(\zeta + \phi_f)}{J_f^{-1}(1 + \zeta\phi_f) + J_m(t)^{-1}(\zeta - \zeta\phi_f)} \right] \qquad (1)$$

where J_c is composite compliance, J_m, matrix compliance, J_f, filler compliance, ϕ_f, filler volume fraction, t, time, and ζ is shape factor which depends on the geometry, orientation and aspect ratio of the particles. Clay is assumed to be time-independent and its compliance, J_f, is taken as 0.0058 GPa^{-1} [10]. Clay volume fraction, ϕ_f, is calculated by discounting the volume occupied by the surfactant which is 55 vol.% in Cloisite® 30B. The parameter ζ is chosen to match the calculated and experimental initial compliances, $J_c(0) = J_0$ at $t = 0$.

Table 2 gives the values for $J_0 = J_c(0)$, ϕ_f and ζ for the PA 6/organoclay nanocomposites (N1.1, N2.2, N3.3 and N4.5) and $J_0 = J_m(0)$ for neat PA 6 (N0.0), while $J_m(t)$ for neat PA 6 (N0.0) is shown in Fig. 5. Thus, predictions of creep compliance $J_c(t)$ of the four nanocomposites using Eq. (1) are superposed in Fig. 5 for the skin/core nanoindentation creep and cantilever-bending creep tests. Also, to examine the time-dependent creep component of each material, the initial compliance, J_0, was subtracted from the creep compliance $J(t)$ and normalized by J_0, as shown in Fig. 6. The predicted curves obtained from Eq. (1) are also plotted in Fig. 6 to compare with the experimental results.

It should be noted that Beckwith's equation describes the behaviour of composites in uniaxial tension, not under the complex stress field created by an indenter. It has also been shown that during the indentation of composites the particles are pushed together, increasing the relative concentration beneath the indenter tip [34]. This means that Beckwith's equation would overestimate the nanoindentation compliance of the composites. However, as evident from Fig. 5a and b, the predicted results according to Eq. (1) either match closely or fall slightly below the experimental data. But more importantly, Fig. 6a and b shows that the time-dependent creep data (minus the effect of J_0) of PA 6/clay nanocomposites are generally *worse* than neat PA 6. These results indicate that organoclay does not have a constraining effect on the polymer chains under nanoindentation and that the observed improvement in creep resistance of PA 6 in Fig. 5a and b is a direct consequence of the much improved initial compliance due to the addition of organoclay.

However, different to the nanoindentation tests, Fig. 6c shows the time-dependent creep data are *reduced* by organoclay under cantilever-bending when compared to neat PA 6, indicating that nanoclay has a constraint effect on the PA 6 chains in this case. The exception being N1.1 in which the organoclay is not fully exfoliated [19]. This means that for effective improvement in bulk creep resistance of PA 6, well-dispersed exfoliated nanoclay is required. Beckwith's equation also overestimates the creep compliance, $J_c(t)$, in Fig. 5c and time-dependent creep in Fig. 6c (except N1.1 which is underestimated). Therefore, it may be inferred that for N2.2, N3.3 and N4.5, organoclay reduces both the initial compliance and the time-dependent creep, which together contribute to the increased creep resistance of these nanocomposites. However,

Fig. 6. Normalized experimental time-dependent creep compliance component of water-saturated PA 6 and its nanocomposites and Beckwith's predictions: (a) nanoindentation on skin region, (b) nanoindentation on core region and (c) cantilever-bending of bulk sample.

for N1.1, the improved creep resistance is solely due to the decrease of the initial compliance. This difference with respect to the other nanocomposites stems from the low degree of exfoliation in N1.1 which yields a higher inter-particle distance and a less dense particle net, allowing the mobility of the polymer molecules and increasing the time-dependent creep.

It is noted that the relative improvement of the bulk and surface creep resistance is not proportional to the organoclay loading. This

is due to the surfactant used to compatibilize the clay which is more compliant than the PA 6 matrix [10] and deteriorates its creep response, as well as the soft γ-crystals [28,29] and small spherulites induced by the organoclay. It is proposed that the lack of evidence of the constraint effect of organoclay in the indentation creep results are due to a combination of the two abovementioned effects (plasticization of the surfactant and morphological changes due to the addition of clay) and the lower capacity of the organoclay to restrict the molecular chain mobility in the surface, which is a direct consequence of the higher degree of freedom of the polymer with respect to the bulk [35].

In this particular PA 6/organoclay system and according to the studied bulk and surface creep behaviour, the optimum organoclay loading is 3.3 vol.%, beyond which there are no significant improvements in the creep resistance.

4. Conclusions

At room temperature, water-saturated PA 6 and its nanocomposites are in the rubbery plateau. In this rubbery state and according to the DMA cantilever-bending tests, organoclay reduces the creep compliance $J_c(t)$ relative to neat PA 6. It is further shown that exfoliated organoclay is effective in decreasing the time-dependent creep component. This fact supports the hypothesis that nanoparticles, unlike their micro-particles counterpart, have a constraint effect on the polymer matrix at the molecular level.

In the nanoindentation tests, the creep compliance was also decreased by the addition of clay. However, it was orchestrated by the reduction in the initial compliance J_0, and not the time-dependent component, indicating that the constraint effect is not evident in the nanoindentation tests. This difference with respect to the results obtained in cantilever-bending is attributed to the higher capacity of organoclay to restrict the molecular mobility in the bulk compared to the surface.

Overall, the addition of organoclay above 3.3 vol.% does not further improve the creep resistance of the nancomposites. This is attributed to the increasing proportion of the soft surfactant in the clay and the modification of the PA 6 morphology upon introduction of the nano-platelets.

Acknowledgements

Appendix A

To determine the creep compliance, J, stepwise load-unload spherical indentations at different creep loads are performed. The analysis of the curves is as follows:

1. The Oliver–Pharr's method [36] corrected by the Ngan–Tang's equation [37] is used to determine the initial compliance, J_0, which is the inverse of the elastic modulus, E.
2. The normalized "apparent" creep compliance, $\frac{J^{app}}{J_0}$, is obtained from the displacement/time curves in the load holding period as:

$$\frac{J^{app}(t)}{J_0} = \left(\frac{h(t)}{h_0}\right)^{3/2}_{spherical} \tag{A-1}$$

where $h(t)$ is displacement during the holding of the load and h_0 is initial displacement at maximum load, i.e., $h(0)$.

3. The plastic displacement ratio, $\frac{h_0^p}{h_0^e}$, is calculated as:

$$\frac{h_0^p}{h_0^e} = h_0 - \left[\frac{3(1-v^2)P_0J_0}{4\sqrt{R}}\right]^{2/3} \bigg/ \left[\frac{3(1-v^2)P_0J_0}{4\sqrt{R}}\right]^{2/3} \tag{A-2}$$

where v is the Poisson ratio of the material, R is the radius of the indenter and P_0 is the load in the holding period.

4. The true normalized creep compliance values, $\frac{J}{J_0}$, are determined from plots $\frac{J^{app}}{J_0}\Big|_{t=t_n}$ vs $\frac{h_0^p}{h_0^e}$ by extrapolating $\frac{J^{app}}{J_0}$ at various loads to zero plastic displacement for each given time, tn, using linear regressions.
5. The creep compliance J is calculated as:

$$J(t) = \frac{J}{J_0}(t) \times J_0 \tag{A-3}$$

References

[1] Ranade A, Nayak K, Fairbrother D, D'Souza NA. Maleated and non-maleated polyethylene–montmorillonite layered silicate blown films: creep, dispersion and crystallinity. Polymer 2005;46(18):7323–33.
[2] Yang J-L, Zhang Z, Schlarb AK, Friedrich K. On the characterization of tensile creep resistance of polymer nanocomposites. Part I: Experimental results and general discussions. Polymer 2006;47(8):2791–801.
[3] Drozdov AD, Hg Lejre A-L, Christiansen J de C. Viscoelasticity, viscoplasticity, and creep failure of polypropylene/clay nanocomposites. Compos Sci Technol 2009;69(15–16):2596–603.
[4] Vlasveld DPN, Bersee HEN, Picken SJ. Creep and physical aging behaviour of PA6 nanocomposites. Polymer 2005;46(26):12539–45.
[5] Cho JW, Paul DR. Nylon 6 nanocomposites by melt compounding. Polymer 2001;42(3):1083–94.
[6] Kim SW, Jo WH, Lee MS, Ko MB, Jho JY. Effects of shear on melt exfoliation of clay in preparation of nylon 6/organoclay nanocomposites. Polym J 2002;34(3):103–11.
[7] Weon J-I, Sue H-J. Effects of clay orientation and aspect ratio on mechanical behavior of nylon-6 nanocomposite. Polymer 2005;46(17):6325–34.
[8] Tamura K, Uno H, Yamada H, Umeyama K. Layered silicate–polyamide-6 nanocomposites: influence of silicate species on morphology and properties. J Polym Sci Part B 2009;47(6):583–95.
[9] Tung J, Gupta RK, Simon GP, Edward GH, Bhattacharya SN. Rheological and mechanical comparative study of in situ polymerized and melt-blended nylon 6 nanocomposites. Polymer 2005;46(23):10405–18.
[10] Vlasveld DPN, Groenewold J, Bersee HEN, Mendes E, Picken SJ. Analysis of the modulus of polyamide-6 silicate nanocomposites using moisture controlled variation of the matrix properties. Polymer 2005;46(26):6102–13.
[11] Vlasveld DPN, De Jong M, Bersee HEN, Gotsis AD, Picken SJ. The relation between rheological and mechanical properties of PA6 nano- and micro-composites. Polymer 2005;46(23):10279–89.
[12] Lee Y-H, Bur AJ, Roth SC, Start PR, Harris RH. Monitoring the relaxation behavior of nylon/clay nanocomposites in the melt with an online dielectric sensor. Polym Adv Technol 2005;16(2–3):249–56.
[13] Weitsman Y. Moisture in composites: sorption and damage. In: Reifsnider KL, editor. Fatigue of composite materials. Amsterdam: Elsevier Science; 1991.
[14] Yao J, Ziegmann G. Equivalence of moisture and temperature superposition in accelerated test method and its application in prediction of long-term properties of glass-fiber reinforced epoxy pipe specimen. Polym Test 2006;25(2):149–57.
[15] Reimschuessel HK. Relationships on the effect of water on glass transition temperature and Young's modulus of nylon 6. J Polym Sci Polym Chem Ed 1978;16(6):1229–36.
[16] Fornes TD, Paul DR. Crystallization behavior of nylon 6 nanocomposites. Polymer 2003;44(14):3945–61.
[17] Yu Z-Z, Yang M, Zhang Q, Zhao C, Mai Y-W. Dispersion and distribution of organically modified montmorillonite in nylon-66 matrix. J Polym Sci Part B 2003;41(11):1234–43.
[18] Shen L, Tjiu WC, Liu T. Nanoindentation and morphological studies on injection-molded nylon-6 nanocomposites. Polymer 2005;46(25):11969–77.
[19] Seltzer R, Frontini PM, Mai Y-W. Effect of hygrothermal ageing on morphology and indentation modulus of injection moulded nylon 6/organoclay nanocomposites. Compos Sci Technol 2009;69(7–8):1093–100.
[20] Seltzer R, Mai Y-W. Depth sensing indentation of linear viscoelastic–plastic solids: a simple method to determine creep compliance. Eng Fract Mech 2008;75(17):4852–62.
[21] Lu H, Wang B, Ma J, Huang G, Viswanathan H. Measurement of creep compliance of solid polymers by nanoindentation. Mech Time-Depend Mater 2003;7(3–4):189–207.
[22] Huang G, Wang B, Lu H. Measurements of viscoelastic functions of polymers in the frequency-domain using nanoindentation. Mech Time-Depend Mater 2004;8(4):345–64.
[23] Tweedie CA, Van Vliet KJ. Contact creep compliance of viscoelastic materials via nanoindentation. J Mater Res 2006;21(6):1576–89.

[24] Kojima Y, Usuki A, Kawasumi M, Okada A, Kurauchi T, Kamigaito O, et al. Novel preferred orientation in injection-molded nylon 6-clay hybrid. J Polym Sci 1995;33(7):1039–45.

[25] Woodward AE, Sauer JA. The dynamic mechanical behavior of some nylons. J Colloid Sci 1957;12(4):363–77.

[26] Pramoda KP, Liu T. Effect of moisture on the dynamic mechanical relaxation of polyamide-6/clay nanocomposites. J Polym Sci Part B 2004;42(10):1823–30.

[27] Zulfiqar S, Ishaq M, Sarwar MI. Effect of surface modification of montmorillonite on the properties of aromatic polyamide/clay nanocomposites. Surf Interface Anal 2008;40(8):1195–201.

[28] Miyasaka K, Isomoto T, Koganeya H, Uehara K, Ishikawa K. Nylon-6 α-phase crystal: chain repeat distance and modulus in the chain direction at low temperature. J Polym Sci Part B 1980;18(5):1047–52.

[29] Tashiro K, Tadokoro H. Calculation of three-dimensional elastic constants of polymer crystals. 3. α and γ forms of nylon 6. Macromolecules 1981;14(3):781–5.

[30] Hbaieb K, Wang QX, Chia YHJ, Cotterell B. Modelling stiffness of polymer/clay nanocomposites. Polymer 2007;48(3):901–9.

[31] Halpin JC. Stiffness and expansion estimates for oriented short fiber composites. J Compos Mater 1969;3(4):732–4.

[32] Chavarria F, Paul DR. Comparison of nanocomposites based on nylon 6 and nylon 66. Polymer 2004;45(25):8501–15.

[33] Beckwith SW. Viscoelastic characterization of a nonlinear, glass/epoxy composite including the effects of damage. PhD thesis, Texas A&M University, Mechanics and Materials Research Center; 1974.

[34] Shen YL, Guo YL. Indentation modelling of heterogeneous materials. Modell Simul Mater Sci Eng 2001;9(5):391–8.

[35] Erichsen J, Kanzow J, Schürmann U, Dolgner K, Günther-Schade K, Strunskus T, et al. Investigation of the surface glass transition temperature by embedding of noble metal nanoclusters into monodisperse polystyrenes. Macromolecules 2004;37(5):1831–8.

[36] Oliver WC, Pharr GM. An improved technique for determining hardness and elastic modulus using load and displacement sensing indentation experiments. J Mater Res 1992;7(6):1564–83.

[37] Ngan AHW, Tang B. Viscoelastic effects during unloading in depth-sensing indentation. J Mater Res 2002;17(10):2604–10.